NUREG/CR-0427
BNL-NUREG-50910
R-7

ACCIDENT PROGRESSION FOR A LOSS OF HEAT SINK WITH SCRAM IN A LMFBR

R.A. BARI, H. LUDEWIG, W.T. PRATT AND Y.H. SUN

Manuscript Completed: October 1978
Date Published: October 1978

ENGINEERING AND ADVANCED REACTOR SAFETY DIVISION
DEPARTMENT OF NUCLEAR ENERGY, BROOKHAVEN NATIONAL LABORATORY
UPTON, NEW YORK 11973

PREPARED FOR
U.S. NUCLEAR REGULATORY COMMISSION
OFFICE OF NUCLEAR REACTOR REGULATION
WASHINGTON, D.C. 20555
CONTRACT NO. EY-76-C-02-0016
FIN NO. A-3000

NOTICE

Available from
U.S. Nuclear Regulatory Commission
Washington, D.C. 20555

Available from
National Technical Information Service
Springfield, Virginia 22161

ABSTRACT

A description of a slow core meltdown in a liquid metal fast breeder reactor is presented for the conditions of loss-of-heat-sink following neutronic shutdown. Simple models are developed for the prediction of phase changes and/or relocation of the core materials including fuel, clad, ducts, control rod absorber material (B_4C), and plenum gases. The sequence of events is accounted for and the accident progression is described up to the point of recriticality. The neutronic behavior of the disrupted core is analyzed in R-Z geometry with a static transport theory code (TWOTRAN). For most scenarios assessed, the reactor is expected to become recritical although large ramp rates are not anticipated.

TABLE OF CONTENTS

TABLE OF CONTENTS (Cont.)

LIST OF TABLES

LIST OF FIGURES

1. INTRODUCTION

1.1 LMFBR Core Disruption

In the final environmental statement[1] by the Nuclear Regulatory Commission on the construction of the Clinch River Breeder Reactor (CRBR) Plant, a hypothetical accident initiated by a loss-of-heat-sink, following (or associated with) a normal scram of the reactor was singled-out as a possible candidate for a core-disruptive accident. The probability of failure of the decay heat removal system to remove long-term decay heat has been addressed by the CRBR applicant[2]. Furthermore, independent studies at BNL[3] have shown that the failure probability of the shutdown heat removal system of the CRBR can be greater than 10^{-6} per year. The potential for a core-disruptive accident in a liquid metal fast breeder reactor (LMFBR) following a loss-of-heat-sink, with scram, is generally recognized[4] and warrants investigation.

A loss-of-heat-sink, following reactor shutdown, has been found to be a significant contributor to risk in commercial light water reactors (LWRs). The Reactor Safety Study[5] found that a core-melt can result from this accident scenario with a likelihood that is comparable to that derived for the loss-of-coolant accident (LOCA) scenarios (the other dominant contributors to risk in the LWR).

For the LMFBR, there is the additional concern that, as a result of a core-melt, core materials can come (in-vessel) into a reconfiguration that can lead to recriticality and consequent energetics. In this context the unprotected loss-of-flow accident and the unprotected transient overpower accident have received much attention in safety analyses. It has been suggested by some authors[6]

that these accidents could lead to a subcritical transition phase of core disruption for which some of the fuel and/or steel is frozen at the axial boundaries of the core, and the remainder of the fuel-steel mixture is in a "boiled-up" state (even at decay heat levels). Chan et al.[7] noted that core disruption phenomena are not limited to these two accident scenarios, and they investigated an alternative core-disruptive accident scenario which led to the possibility of recriticality. Chan et al.[7] have concluded, independently from us, that recriticality may occur (for a particular loss-of-heat-sink accident, with scram) as a result of a gradual meltdown of core steel and collapse of nonmolten fuel pellets.

This work describes a study of possible accident sequences following a loss-of-heat-sink during normal reactor shutdown in a LMFBR. Design information for the CRBR has been used in the specific analysis carried out. The accident proceeds from the assumptions that 1) a normal shutdown has occurred and 2) all heat removal capabilities have failed, including natural convection. Detailed accounts of parts of this work have appeared elsewhere: an analysis of the meltdown phase of the accident is given in Reference 8, and an analysis of material relocation and recriticality is given in Reference 9. Furthermore, brief accounts of these works are presented in American Nuclear Society Transactions[10, 11].

In the work of Chan et al.[7], it was postulated that the accident was initiated by sudden ruptures of all pipes connected to the reactor vessel (with scram). The sodium heat-up and boil-off processes were then analyzed in some detail. In the present work, it was assumed that the primary heat transport system remained intact initially during shutdown, but that there was no heat rejected from the primary coolant system through the heat

exchangers. Here, it is postulated that the ultimate heat sink (water supply or air blast heat exchangers) fails, but that pony motor flow rate is maintained in the adiabatic primary sodium heat transport system. Gradually, the primary system sodium temperature will both increase and become more uniform. It is then postulated that electric power is lost to the pony motors.

The boiling dynamics of sodium was not addressed in detail, but it was determined (in agreement with Reference 7) that sustained dryout of the cladding was required for meltdown. Clearly, this situation will eventually occur for the scenario postulated here. Thus, in the present work, the analysis begins at the point at which the sodium uniformly reaches the saturation temperature and the primary heat transfer system is adiabatic.

1.2 Scope of Work

If boiling can be sustained and eventually leads to clad dryout, then clad and fuel melting must also be considered. The problem then becomes that of predicting clad and fuel relocation with the eventual aim of establishing probable core meltdown configurations. Analysis of this problem is complicated, not only by its complexity, but also by the long transient times involved in the various accident phases.

The analysis of a problem of this complexity may be conducted with varying degrees of rigor. Initially, to obtain an indication of the magnitude of the times involved in the various accident stages, a simple heat capacity approach was adopted. The heat capacity approach is described in Reference 8, and the results of simple hand calculations were found to be in reasonable agreement with alternate and more sophisticated methods that were used for describing the heat-up stages of the accident.

It was found, however, that this simple approach does not adequately describe those stages of the accident in which phase change or material relocation occur. The hand calculations were also tedious and did not readily allow scoping studies to be carried out. It therefore became apparent that a fast running computer code was necessary. The REACTOR subroutine of the DEMO code[13] was chosen as a basis, because of its relatively simple lumped parameter modeling, which could be modified and developed for this purpose. The modified version of the REACTOR subroutine was renamed ALOHA and a description of the code and the data obtained from it are included in Reference 8. The ALOHA code was particularly useful for scoping studies and for validating some of the assumptions made in the heat capacity approach. In view of the close agreement between the predictions of the heat capacity model and the ALOHA code, it was decided to use the simpler heat capacity model as a basis for material relocation.

A computer code, LOHS, was therefore developed to solve the heat capacity model described in Reference 8, and more fully in Section 2.1.2 of this work. The LOHS code is faster running than ALOHA and it allowed easier coupling of the relocation model. The error involved in using the simpler modeling in the LOHS code, compared with, ALOHA is minimal.

The relocation model developed was described in Reference 8, and due to the simplicity of the computations, a small stand-alone code, CLAD, was written at that time. Preliminary data from CLAD was given in Reference 8 and the results of a sensitivity study were presented in Reference 9. This model, which is described in Section 2.2, was coupled to the heat-up code LOHS through the RLOCATE subroutine.

Failure of the cladding on the fuel or control pins before the beginning of the melt phases is an important possibility in the accident scenario. The role of high He gas pressure in the B_4C control pins as a mechanism for clad and/or pellet failure is discussed in Sections 3.1 and 3.2. An assessment of the premelt failure of the fuel pin pellets is given in Section 3.3.

The potential for recriticality was assessed for various collapsed core configurations which seemed plausible. The calculations were done in time-independent transport theory in two-dimensional R-Z geometry.

1.3 Major Conclusions

The single major conclusion of this work is that recriticality will occur for the postulated forced meltdown (starting from shutdown conditions) of the CRBR core. This conclusion is based on the crucial assumption that sustained dryout of the fuel cladding occurs and that sodium does not re-enter the core space for approximately twenty minutes at a decay power level of approximately one percent of full power.

Recriticality occurs for a broad range of likely relocation patterns of fuel, absorber and stainless steel, and the ramp rate is on the order of (or less than) 100 \$/m of slumping material. Furthermore, only if the material compacts at a free-fall velocity, then would the resulting ramp rate be on the order of 100 \$/s. However, for the accident scenarios considered, the core disruption process is rather slow and sluggish and, therefore, much smaller ramp rates ($\leq$ 10 \$/s) are anticipated.

2. METHODS OF ANALYSIS

Since the problem involves very slow transients, the mathematical models developed to describe the various accident stages were purposely made simple so that the accident sequence could be analyzed within reasonable computing times. Initially, it was necessary to analyze the heating processes in the core and the methods adopted are discussed in Section 2.1. When the melt phases are reached, material relocation must be considered. Downward relocation is expected because of the low sodium vapor velocities encountered at the decay power levels under consideration. A simple melting and freezing (downward) relocation model has been developed and is described in Section 2.2. The processes associated with relocation of fuel and absorber materials are discussed in Section 3. Finally, as material relocation occurs, the potential for recriticality has to be assessed and the computational technique used in the assessment is discussed in Section 2.3.

2.1 Heat-up Processes

The starting point for the present analysis was discussed in Section 1.1, and begins with the assumption of sustained dryout in the fuel assemblies. The boiling dynamics of the sodium was not addressed in detail, however, it is important to estimate the time to reach sustained dryout after shutdown. The time-to-dryout establishes the point on the decay heat curve at which the fuel pins begin to heat-up and eventually meltdown. The methods used to establish the time to sustained dryout are discussed in Section 2.1.1.

After clad dryout, the heat-up of the core must be predicted. The simplest approach is to assume that the times to the various events are functions only of

the heat generation and the heat capacities of the materials in the subassemblies, and any latent heats of vaporization or fusion that may have to be overcome during the temperature interval of interest. This heat capacity approach is discussed in Section 2.1.2 and is in reasonable agreement with alternate and more sophisticated methods[8].

2.1.1 Preboiling Heat-up Phase

An estimation of the sodium heat-up rate, assuming that the primary sodium heat transport system is adiabatic at shutdown, was made at BNL[12] using the DEMO code[13]. No heat was rejected from the primary sodium circuit through the heat exchangers, and circulation continued under pony motor flow. The temperature response of various regions of the primary sodium circuits, as predicted by DEMO, are shown to 2000 seconds after shutdown in Figure 1. Clearly, the sodium temperatures in the primary circuit are rapidly converging at 2000 seconds.

In Reference 12, a simple lumped parameter heat capacity model was used to predict the heat-up of sodium in the adiabatic primary circuit and the temperature predicted at 2000 seconds was found to be within one percent of the bulk average temperature computed by the DEMO code (Figure 1). In view of the close agreement between the two approaches, the lumped parameter method was used to extrapolate the DEMO data out to the sodium saturation temperature. The bulk sodium temperature was found to approach saturation after $\sim$ 12000 seconds. The decay power level at 12000 seconds is $\sim$ 1.3% of full power.

The sensitivity of the sodium heat-up time in the Fast Flux Test Facility to the time the heat sink is lost after shutdown was examined in Reference 12. Renormalizing the data presented in Reference 12 to the CRBR implies that

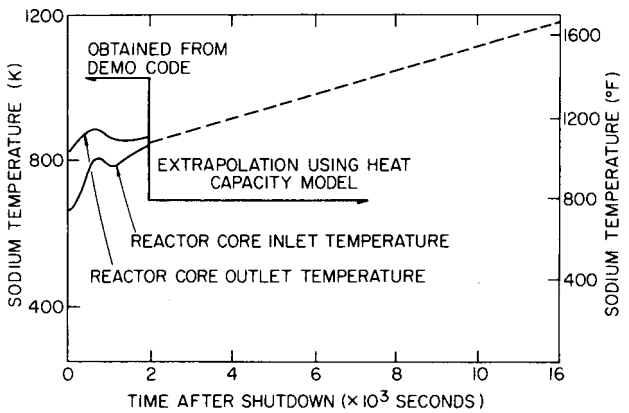

Figure 1. Temperature response assuming an adiabatic primary sodium heat transport system.

(under the adiabatic primary circuit assumption) the bulk of the primary sodium would reach saturation at decay power levels between 1.3% and 0.9% of full power. The post-dryout heat-up calculations presented here are therefore based on a nominal decay power level of 1% of full power. The sensitivity of the meltdown to variations in the decay power level after dryout was considered in Reference 8 using the ALOHA code.

2.1.2 Post-Dryout Heat-up Phase

Initially, it was necessary to select a representative subassembly configuration to simplify the heat transfer calculations. Since the relative movement between fuel and control assemblies is of particular interest, the configuration shown in Figure 2 was selected as representative of the proposed CRBR core design. Other regions were examined (i.e., the radial blanket) but the heat-up times were found to be an order of magnitude slower than for the active core. The subassembly array consists of a control assembly surrounded by six average fuel assemblies. Heat transfer between adjacent fuel assemblies was considered only as far as the intersubassembly sodium (see Figure 2), and then only during the convective and boiling regimes. It was assumed, after dryout of the intersubassembly sodium, that adjacent fuel assembly duct walls were at the same temperature so that there was no net transfer of thermal radiation. However, heat transfer into the control assembly was considered during all stages of the accident. It was also assumed that radial heat transfer would be dominant, and thus axial heat transfer along fuel pins was neglected.

The application of the heat capacity approach begins with the assumption of sustained dryout in the fuel assemblies so that only the subsequent heating of the fuel pins and the heat transfer to the adjacent control assemblies must be considered. If the heat transfer is also assumed symmetrical about each of the six surfaces of the central control assembly (Figure 2), then the simple average pin nodalization shown in Figure 3 can be used.

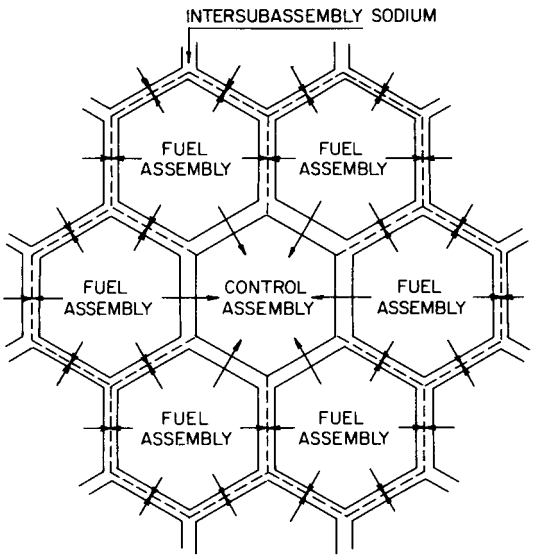

Figure 2. Seven subassembly array model.

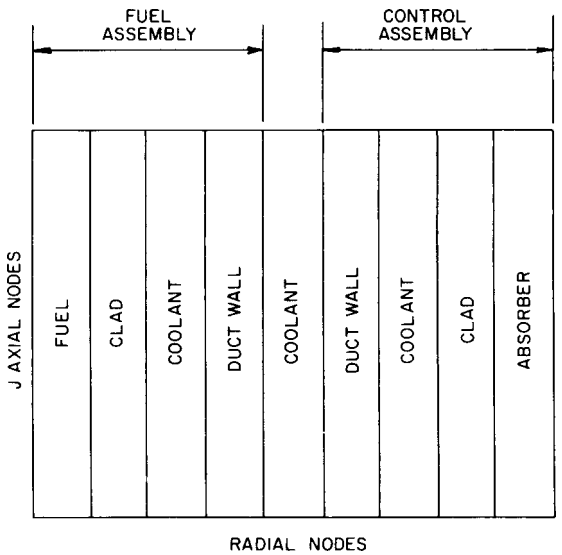

Figure 3. Nodalization scheme.

A time-dependent energy equation can be written for the fuel pins in terms of the internal decay heat Q_{INT} and heat lost by radiation Q_R, which describes heating of the pins up to the point of clad melting:

$$(M_F\ C_{PF} + M_{FC}\ C_{PFC})\ \frac{\partial T_F}{\partial t} = Q_{INT} - Q_R \qquad (2.1)$$

The above equation neglects convective heat transfer from the fuel pins to the sodium vapor. This assumption is reasonable at the low vapor velocities experienced in this investigation. The radiation heat loss Q_R is based on a steady-state analysis of radiative heat transfer from the fuel pins of a voided subassembly to a coolable duct wall, which was reported by Chan et al.[14]. The radiative heat transfer model is discussed in detail in Section 2.1.3. The lumped heat capacity model (Equation 2.1) neglects heat transfer between the fuel and the cladding. This implies that the fuel pellet temperature is equal to the cladding temperature, which for very slow transients is a reasonable assumption. Equation 2.1 is solved in a stepwise manner by applying the following approximate equation at each time step:

$$T_F\ (t + \Delta t) = T_F\ (t) + \frac{\Delta t\ (Q_{INT} - Q_R)}{(M_F\ C_{PF} + M_{FC}\ C_{PFC})} \qquad (2.2)$$

For a given temperature difference between fuel and duct wall at the beginning of a time step, a thermal radiative heat loss Q_R is calculated and subtracted from the fuel decay heat, Q_{INT}. The difference is then used to calculate the temperature rise over the next time step.

When the cladding reaches its melting point, the difference between fuel decay heat and the thermal radiative heat loss is assumed to go to

melting the steel. The amount of steel melted in any time step Δt is therefore given by the following approximate equation:

$$\Delta M_{FC} = \frac{(Q_{INT} - Q_R)}{\lambda_{FC}} \Delta t \tag{2.3}$$

After all of the clad has been melted and relocated, the exposed fuel pellets are then free to heat-up and the temperature rise is predicted by the following approximate expression:

$$T_F\ (t + \Delta t) = T_F\ (t) + \frac{\Delta t}{M_F\ C_{PF}}\ (Q_{INT} - Q_R) \tag{2.4}$$

The radiative heat transfer from the fuel to the duct wall will boil-off the intersubassembly sodium (during this period the fuel duct is assumed to be isothermal with the intersubassembly sodium at the latter's saturation temperature). The sodium boil-off rate is given by:

$$\frac{\partial M_{BOIL}}{\partial t} = \frac{Q_R}{h_{fg}} \tag{2.5}$$

After dryout of the intersubassembly sodium, the fuel duct wall is free to heat-up and the temperature rise can be predicted by the following approximate expression:

$$T_{FD}\ (t + \Delta t) = T_{FD}\ (t) + \frac{\Delta t}{M_{FD}\ C_{PFD}}\ (Q_R - Q_R') \tag{2.6}$$

After dryout of the intersubassembly sodium, the heat exchange between the fuel assembly duct wall and the control assembly duct wall Q_R' is based on

radiative heat transfer between parallel flat plates assuming the emissivity of the stainless-steel duct wall to be 0.7 as suggested by Chan et al.[14]. It is recognized that the emissivity of the duct walls vary with temperature and surface conditions, however, such variations were found not to strongly influence the overall accident progression. Heat transfer, by thermal radiation between the fuel and control assembly duct wall, occurs for a relatively short period ($\sim$ 5 minutes) and is small compared with thermal heat transfer directly from the fuel pins. Variations in the assumed emissivity of the steel does not therefore significantly alter our estimate of the post-dryout, heat-up phase presented in Section 4.1.1.

When the fuel assembly duct wall reaches its melting point, all of the heat remaining in the duct wall is assumed to melt the steel. The amount of steel melted at any time Δt is therefore given by the following approximate equation:

$$\Delta M_{FD} = \frac{(Q_R - Q_R')}{\lambda_{FD}} \Delta t \qquad (2.7)$$

After meltdown of the fuel assembly duct wall, the radiative heat loss of the fuel pins Q_R is transferred directly to the control assembly duct wall. Initially, all of the radiative heat transfer to the control assembly duct wall is assumed to boil the sodium in the control assembly. If the fuel assembly duct wall remains intact, then the sodium boil-off rate in the control assembly is given by:

$$\frac{\partial M_{BOIL}}{\partial t} = \frac{Q_R'}{h_{fg}} \qquad (2.8)$$

However, if the fuel assembly duct wall has melted, then the sodium boil-off rate in the control assembly is given by Equation 2.5.

After dryout of the control assembly sodium, the control assembly duct wall is free to heat-up and the equation for the temperature rise depends on whether or not the fuel assembly duct wall has melted:

With intact fuel assembly duct wall:

$$T_{CD}\ (t + \Delta t) = T_{CD}\ (t) + \frac{\Delta t}{M_{CD}\ C_{PCD}}\ (Q'_R - Q''_R) \qquad (2.9)$$

Here Q" is the radiative heat exchange between the control duct wall and the control pins.

With melted fuel assembly duct wall:

$$T_{CD}\ (t + \Delta t) = T_{CD}\ (t) + \frac{\Delta t}{M_{CD}\ C_{PCD}}\ (Q_R - Q''_R) \qquad (2.10)$$

After meltdown of the control assembly duct wall, the radiative heat loss from the fuel pins Q_R is transferred directly to the control pins. When the control assembly duct wall reaches its melting point, all of the heat remaining in the duct wall is assumed to melt the steel. The amount of steel melted at any time step Δt is given by:

$$\Delta M_{CD} = \frac{(Q_R - Q''_R)}{\lambda_{CD}}\ \Delta t \qquad (2.11)$$

After dryout of the control assembly sodium, the control pins are free to heat-up and the equation for the temperature rise of the pins depends on whether or not the control assembly duct wall has melted:

With an intact control assembly duct wall:

$$T_C\ (t + \Delta t) = T_C\ (t) + \frac{\Delta t\ Q''_R}{(M_{CC}\ C_{PCC} + M_C\ C_{PC})} \qquad (2.12)$$

With a melted control assembly duct wall:

$$T_C\ (t + \Delta t) = T_C\ (t) + \frac{\Delta t\ Q_R}{(M_{CC}\ C_{PCC} + M_C\ C_{PC})} \tag{2.13}$$

When the control pin cladding reaches its melting point, all of the radiative heat transfer to the pins is assumed to melt the steel. The amount of steel melted at any time step Δt is given by:

$$\Delta M_{CC} = \frac{Q_R}{\lambda_{CC}}\ \Delta t \tag{2.14}$$

After all the control pin clad has melted and relocated, the exposed absorber material is then free to heat-up and the temperature rise is given by:

$$T_C\ (t + \Delta t) = T_C\ (t) + \frac{\Delta t\ Q_R}{M_C\ C_{PC}} \tag{2.15}$$

Melting of the fuel and absorber material is predicted to occur at approximately the same time (Section 4.1). The meltdown of the fuel can be predicted using an equation similar to Equation 2.3 with the appropriate latent heat of fusion, whereas the meltdown of the absorber material can be predicted by Equation 2.14, also with the appropriate latent heat of fusion. The direct radiation heat transfer between the fuel and absorber pins depends on the relative meltdown position of the two materials.

The heat capacity approach discussed above is simple to apply, however, as extensive computations were required, a simple computer code, LOHS, was developed to solve the set of equations. A flow diagram for the code is shown in Figure 4. The flow diagram is self-explanatory and the heat-up calculations are carried out in the main part of LOHS. The subroutine, INPUT, allows the

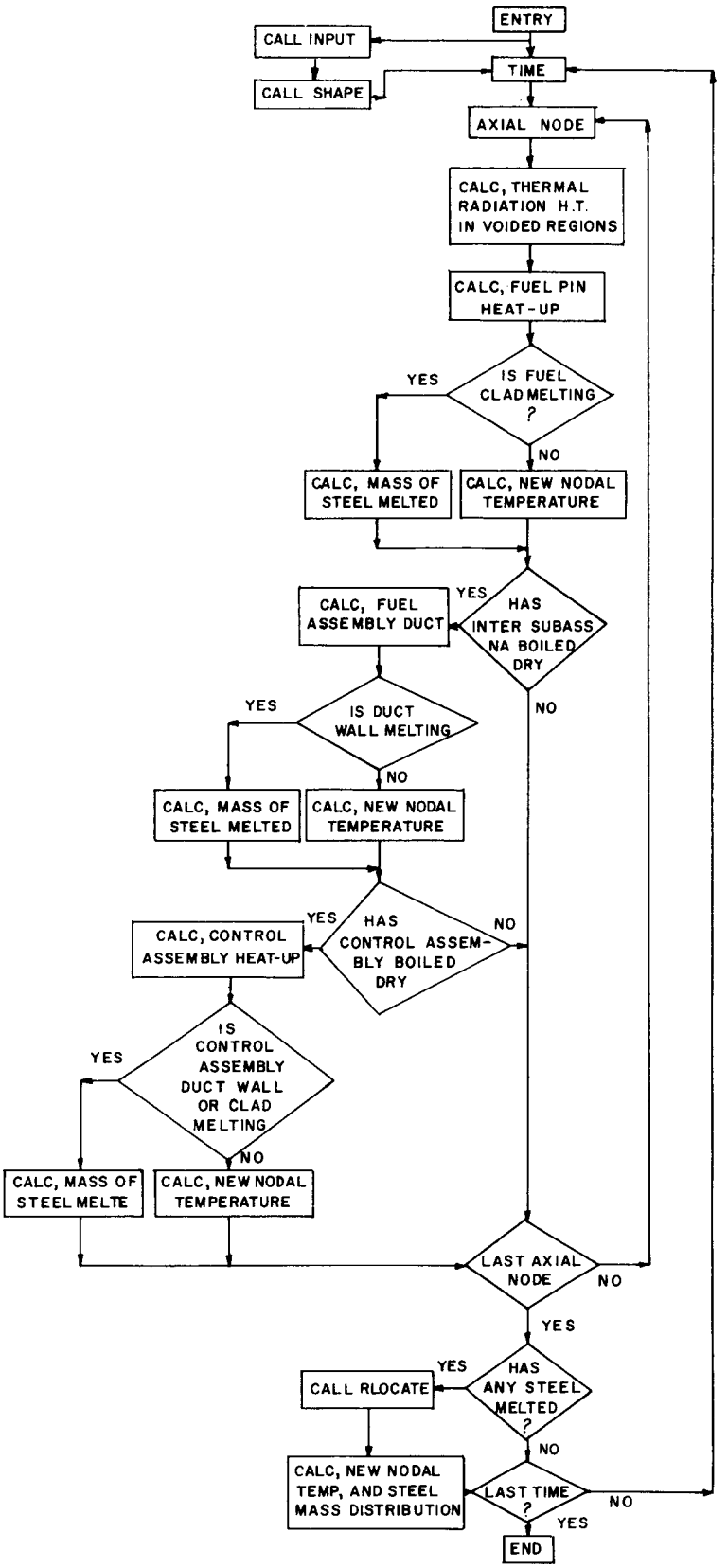

Figure 4. Flow diagram for LOHS.

user to specify the number of axial nodes and subroutine, SHAPE, calculates the axial nodal power profile. The heat-up computations described above cannot account for material relocation during meltdown, so that a relocation model was developed (also based on a heat capacity approach). The relocation model is discussed in Section 2.2 and was coupled to the LOHS code through the subroutine, RLOCATE.

2.1.3 Subassembly Thermal Radiation

After clad dryout occurs in the fuel assemblies, thermal radiation becomes a dominant heat transfer mechanism. A steady-state analysis of radiative heat transfer from the fuel pins of a voided subassembly to a coolable duct wall has been reported by Chan et al.[14]. The surface-to-surface radiative exchange among pins was analyzed by exact Ring-to-Ring and Pin-to-Pin models and by an approximate cylindrical Ring-to-Ring model. Good agreement was obtained between the models for the steady-state case of equal power generation in each pin with a uniform duct wall temperature.

The situation is rather more complicated in the present analysis due to the transient nature of the radiative exchange. Immediately after dryout in the fuel assembly, the fuel pin temperature will be close to the duct wall temperature, resulting in negligible thermal radiation. However, as the fuel pins heat-up after clad dryout, the duct wall will remain, for a time, coolable due to the presence of intersubassembly sodium. The increased temperature difference results in significant thermal radiation. After dryout of the intersubassembly sodium, the temperature of the fuel duct wall is then free to rise. This will continue until the cladding begins to melt. The cladding will melt at constant temperature but the duct wall temperature is free to rise. After the cladding

melts, the fuel will continue to heat-up as will the duct wall until it in turn begins to melt. Melting of the duct wall is also at constant temperature. The process then continues into the control assembly.

Clearly, a radiative heat transfer problem of this complexity requires simplification before it can be analyzed as a part of the present accident scenario. If the simplest of Chan's steady-state models is selected, then the hexagonal rings of pins in a fuel subassembly are represented by annular rings, each with a volume equivalent to that of the pins in the respective ring. Chan et al.[14] assume that each surface is black (i.e., emissivity of unity) and sees only one other black surface besides itself. With these assumptions, Chan relates the thermal radiative heat flux q_R to the maximum fuel pin temperature T_F and duct-wall temperature T_{FD} through the following equation:

$$q_R \sum_{i=1}^{N-1} \frac{1 + 3i(i-1)}{1 + \delta\,(i-1)} = \sigma\,(T_F^4 - T_{FD}^4) \qquad (2.16)$$

It may be noted that the expression $1 + 3i(i-1)$ in the above equation is simply the total number of pins contained inside and including ring i. N is the total number of rings considered and δ equals the pitch of the rings divided by a fuel pin radius. The temperatures of the intermediate fuel pin rings can be obtained from generalized forms of the above equation.

The heat lost by radiation Q_R from the fuel pins to the duct wall can be related to the thermal radiative heat flux q_R through the following equation:

$$Q_R = Aq_R = \sigma AK\,(T_F^4 - T_{FD}^4) \qquad (2.17)$$

$$\text{in which } K = 1/\sum_{i=1}^{N-1} \frac{1 + 3i(i-1)}{1 + \delta\,(i-1)}$$

(K = 1/50.39 for CRBR)

Equation 2.16, which is expressed in terms of the maximum fuel temperature, implies a temperature gradient across the assembly. The generalized form of Equation 2.16 can be used at any time step to obtain the temperature gradient between central and outer fuel rings. The temperature gradient across the fuel rings can be related to an average temperature pin, which can in turn be related to the average pin model used in the LOHS code. In a previous BNL report[8], it was found that the temperature gradient across the assembly results in meltdown of the cladding on the central fuel pins well before the outer rings reach the steel melt temperature. An assessment was made of the effect of such incoherency on the overall accident progression and it was determined that all of the steel will be melted from the core region before either the fuel or absorber material reach their respective melt temperature. The meltdown progression reported in Section 4.1.1, which is based on the average pin model, is therefore qualitatively correct.

2.2 Clad and Duct Wall Relocation

Clad will eventually melt at about 5 minutes after dryout, assuming the reactor to be at 1% of full power. The fuel and control assembly duct walls are predicted to melt after several more minutes. The relocation of the molten clad is of particular interest and has been addressed in many publications. It is of particular importance to estimate the preferred direction of relocation. The potential exists for sodium vapor to cause upward relocation of cladding. The sodium vapor velocity can be estimated from a simple energy balance written for the void:

$$u_v = \frac{q\, A_H}{\rho_v\, h_{fg}\, A_f} \tag{2.18}$$

in which q is the heat flux over the heated area A_H and A_f is the flow area of the coolant channel. The above expression predicts a vapor velocity of approximately 10 m/sec at 1% decay power level, which is below the suggested critical flooding velocity for clad and sodium vapor[15]. This implies, for 1% decay power levels, that only downward relocation clad must be considered. Again, because of the long transient times involved, it was necessary to simplify the modeling for this assessment. The model developed is nonmechanistic and is illustrated in Table I. At each time step the generalized heat balance is applied at each axial node. If the node is at a temperature T_j below the melt temperature (nodes 4 and 5, Table I), then a new nodal temperature T_j' is determined. If, however, a node is at the melt temperature (nodes 2 and 3) then the nodal temperature is held constant and the heat remaining in the node is used to melt a fraction of the clad. These calculations are carried out in the main part of the LOHS program. The RLOCATE subroutine simply takes the quantity of clad melted at any given node and relocates it into the node immediately below. The procedure continues until molten material is relocated into a node (node 1), which is below the melt temperature. Under these circumstances, an instantaneous energy balance is carried out and some solidification of the molten material occurs. If the heat necessary to raise the node to the melt temperature, $M_j\ C_{pj}\ (T_m - T_j')$ is greater than the available latent heat of the molten material $\lambda\Delta M_{j+1}$, then all the molten material solidifies and a new nodal temperature is calculated:

$$T_j'' = \frac{M_j\ C_{pj}\ T_j' + \Delta M_{j+1}\ (\lambda + T_m\ C_{pj+1})}{M_j\ C_{pj} + \Delta M_{j+1}\ C_{pj+1}} \qquad (2.19)$$

This temperature will be higher than the temperature T_j' calculated in the main part of the LOHS code, because of the heat released by the solidifying clad.

Table I

Melting and Freezing Relocation Model

AXIAL NODES	TEMPERATURE AT START OF TIME STEP	MELTDOWN DURING TIME STEP	RELOCATION AT END OF TIME STEP	CONDITIONS AT THE START OF THE NEXT TIME STEP
5	$T_5 < T_m$	NO MELTING, HENCE TEMP RISE CALC ΔT_5	NO RELOCATION INTO THIS NODE	NEW NODAL TEMP: $T_5' = T_5 + \Delta T_5$ SOLID MASS: $M_5' = M_5$
4	$T_4 < T_m$	NO MELTING, HENCE TEMP RISE CALC ΔT_4	NO RELOCATION INTO THIS NODE	NEW NODAL TEMP: $T_4' = T_4 + \Delta T_4$ SOLID MASS: $M_4' = M_4$
3	$T_3 = T_m$	MELT FRACTION CALCULATED ΔM_3	NO RELOCATION INTO THIS NODE	NEW NODAL TEMP: $T_3' = T_m$ SOLID MASS: $M_3' = M_3 - \Delta M_3$
2	$T_2 = T_m$	MELT FRACTION CALCULATED ΔM_2	MASS RELOCATION ΔM_3	NEW NODAL TEMP: $T_2' = T_m$ SOLID MASS: $M_2' = M_2 - \Delta M_2$ LIQUID MASS: ΔM_3
1	$T_1 < T_m$	NO MELTING, HENCE TEMP RISE CALC ΔT_1 $(T_1' = T_1 + \Delta T_1)$	MASS RELOCATION ΔM_2	IF $\lambda \Delta M_2 < M_1 C_p (T_m - T_1)$ NEW NODAL TEMP: T_1'' $(T_m > T_1'' > T_1')$ SOLID MASS: $M_1' = M_1 + \Delta M_2$ LIQUID MASS IS ZERO IF $\lambda \Delta M_2 > M_1 C_p (T_m - T_1)$ NEW NODAL TEMP: T_1'' $(T_1'' = T_m)$ SOLID MASS: $M_1' = M_1 + S_1 M_2$ LIQUID MASS: $M_2 - S_1 M_2$

If, however, $M_j C_{pj} (T_m - T_j') < \Delta M_{j+1}$, then the node temperature is put equal to the melt temperature and a fractional solidification S_j is computed:

$$S_j = \frac{M_j C_{pj} (T_m - T_j')}{\lambda \Delta M_{j+1}} \tag{2.20}$$

The material remaining in the molten state is then obtained simply by computing the difference. The procedure is repeated for subsequent time steps and an inventory of the molten and solidified material is maintained. However, a check must be made at each time step on any buildup of material within a node. A simple criterion is used to determine when plugging occurs. As mentioned previously, the relocation model is coupled to the main LOHS program through the subroutine RLOCATE and a flow diagram of RLOCATE is included in Figure 5. This model was applied only to clad or duct wall relocation. A discussion of premelt relocation of both the fuel and absorber material is included in Section 3. The application of the simple model described above to material melting, relocation and freezing is open to question. In particular, the computational procedure is such that the effective relocation speed can be varied simply by varying the axial node size or the magnitude of the time step. A rough estimate of the relocation velocity can be obtained by considering the clad to fall under the influences of gravity and the shear stress between the molten and solid cladding. In this case, velocities on the order of 0.3 m/sec are predicted. In order to assess the impact of the relocation speed on the time to plugging, a range of speeds was considered by using various combinations of node size and time step in a previous BNL report[9]. The results of the sensitivity study indicated that, provided the node size and time step are sufficiently small, the time to and the position of the plug are relatively insensitive to relocation speed.

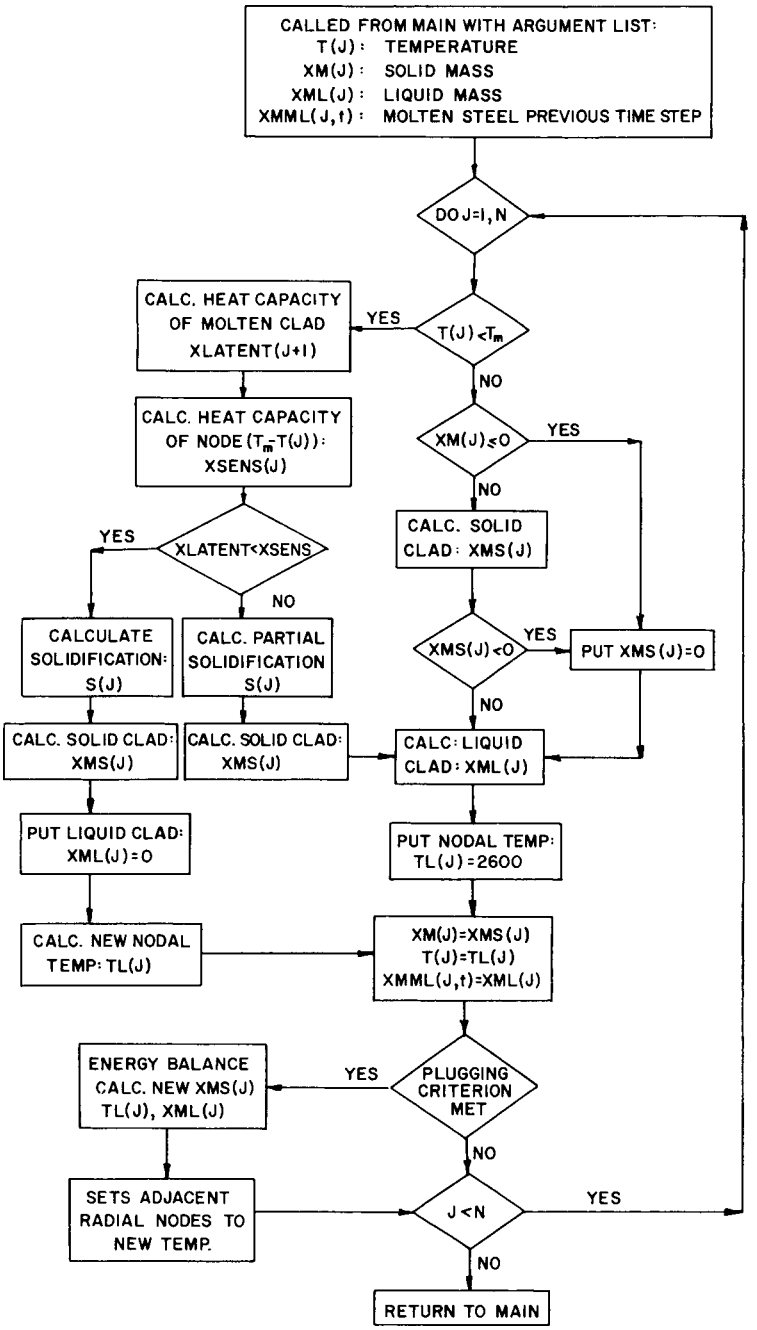

Figure 5. Flow diagram for subroutine RLOCATE.

2.3 Recriticality Analysis: Calculational Technique

The calculational technique used in this analysis is the same as that used in determining the base case configuration[16]. Briefly, this procedure is based on ENDF/B-IV nuclear data and one- and two-dimensional spatial calculations. A 50-group[17] microscopic cross-section library, which is based on ENDF/B-IV and processed by the MINX[18] code, is used as a starting point for the nuclear data. The data in this form is further processed by the CINX code[19] to make its format compatible with the one-dimensional diffusion theory code 1-DX[20]. The 1-DX code is used to collapse the 50-group structure to a 9-group macroscopic cross-section library. In constructing this group structure, an effort was made to confine the threshold reactions primarily to the first macroscopic group, with a small contribution in the second group. Furthermore, the resonance in sodium at approximately 2.85 kev is confined to group 6.

The one-dimensional calculations are carried out either for single zones or for combinations of adjoining zones. In this way, the spectral shifts that occur across zone boundaries can be accounted for in preparing the collapsed cross-section sets. Two-dimensional calculations were carried out in transport theory using R-Z geometry. The TWOTRAN[21,22] code was used for these calculations together with the 9-group library prepared by the methods outlined above.

3. CONTROL AND FUEL ASSEMBLIES PREMELT FAILURES

During a loss-of-heat-sink accident, gases in the fuel and control rod gas plena can be heated and pressurized. This gas pressurization could break the cladding wall and release gases into the coolant channels. The possible timing for cladding rupture is assessed in Section 3.1. The effect of gas release from the gas plenum is evaluated in Section 3.2.

The relocation of fuel and control materials could have a strong effect on the recriticality assessment. Events which may result in fuel and control material relocations are discussed in Sections 3.3 and 3.4. These events include loss of fuel strength, toppling, and control material fragmentation.

3.1 Gas Plenum Depressurization

3.1.1 Control Assemblies

The reaction of neutrons with the control material results in the production of Helium gas in the matrix of the absorber. The axial dependence of the burn-up profile is obtained from Reference 23. The amount of Helium gas released to the gas plenum during normal operation can be determined by:

$$N_{gas} = \pi R^2 \sum_j (C)_j \, (RL)_j \, (\Delta Z)_j \qquad (3.1)$$

where j: jth axial section of the absorber column

R: radius of absorbed column

$(\Delta Z)_j$: length of the jth section

$(C)_j$: neutron captures in the jth section

$(RL)_j$: fractional gas release in the jth section.

In Equation 3.1, both $(C)_j$ and $(RL)_j$ are dependent on the withdrawal history of the control rods during normal operation. For control rods of the first equilibrium cycle core, $(C)_j$ can be determined from Figure 6;

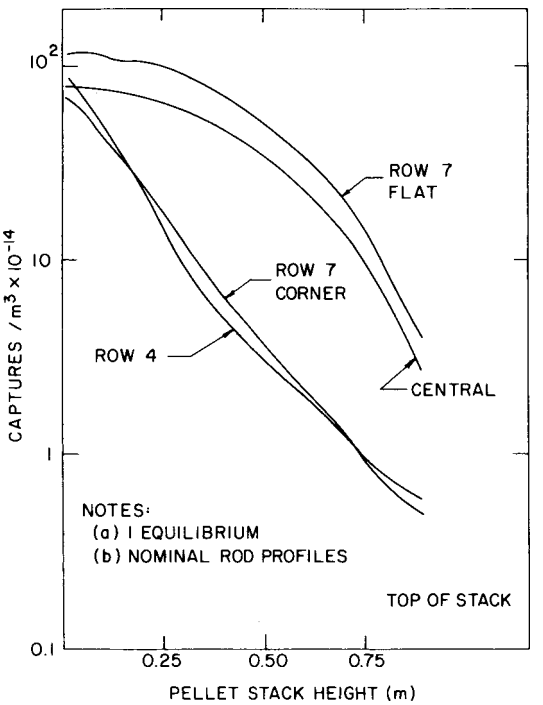

Figure 6. Primary control rod axial burnup profile.

$(RL)_j$ can be determined from the following[24]:

$$(RL)_j = A_j \left[1.32 - 0.032 \left(\frac{C}{10^{20}}\right)_j + 5.9\times10^{-4} \left(\frac{C}{10^{20}}\right)^2_j\right] \quad (3.2)$$

where $A_j = 18.9 \exp - \left(\frac{8990}{T^a_j + 460}\right) + 0.37 \exp \left[(-0.18) \left(\frac{1.8\ T^a_j - 1308}{100}\right)^2\right]$

T^a_j = average temperature (^oC) of the jth section

By using Equations 3.1 and 3.2, the amount of gas released to the gas plenum can be determined for control rods of the first equilibrium cycle.

During the loss-of-heat-sink accident, pressure in the gas plenum increases with increasing temperature. It is evaluated that, for rods of the central and Row 7 flat control assemblies of the first equilibrium cycle core, the gas pressure in the gas plenum can be large enough to break the clad wall before boiling of the coolant in the control assembly. For rods of Row 4 and Row 7 corner assemblies, the clad wall failure can occur during or somewhat before bulk boiling of the coolant.

3.1.2 Fuel Assemblies

The amount of gas released to the gas plenum of fuel pins depends on operating conditions, (i.e., linear power and burnup). It is evaluated in Reference 25 that, for high linear power pins with higher burnup ($\sim$ 8% at.), the pressure in the gas plenum is around 4.83×10^3 KN/m^2 (700 psi). With this pressure in the gas plenum, it can be shown by using the perfect gas law, that the cladding can be ruptured during or before the coolant boils in the fuel assembly.

3.2 Early Gas Release from Gas Plenum

Since the cladding may be ruptured by the plenum pressure during or before the coolant bulk boiling phase occurs, the pressurized plenum gas may thus be released and void the coolant channels. The importance of the heat transfer variations, due to the coolant channel voiding during this gas release process, was considered previously in Reference 8. It was determined that the gas release could not cause voiding for a long enough time to have a significant effect on the heat transfer pattern in the coolant channels.

3.3 Fuel Material Collapse

3.3.1 Fuel Strength Assessment

The purpose of the calculation in this section is to evaluate the possibility of fuel slumping under compression caused by the weight of the above-core fuel assembly structure. The weight of the above-core structure could be transmitted to the fuel columns either through the springs in the upper plenum, or directly by the solid clad if the fuel-clad gap is closed.

According to Byron's compression experiment,[26] the yield stress of uranium dioxide drops with increasing temperature (Figures 7 and 8). As the temperature approaches 2273 K, the yield stress drops sharply - it is about 5.86×10^4 KN/m^2 (8.5 ksi) at 2073 K and only about 1.03×10^4 KN/m^2 (1.5 ksi) at 2273 K. The material loses its strength quickly around this temperature. This result is consistent with Bard's results[27] (Figure 8) where the material strength (represented by Young's Modulus) drops sharply at a temperature also near 2273 K.

As the fuel temperature increases, the high temperature creep can soften the fuel material and significant plastic deformation can be induced.

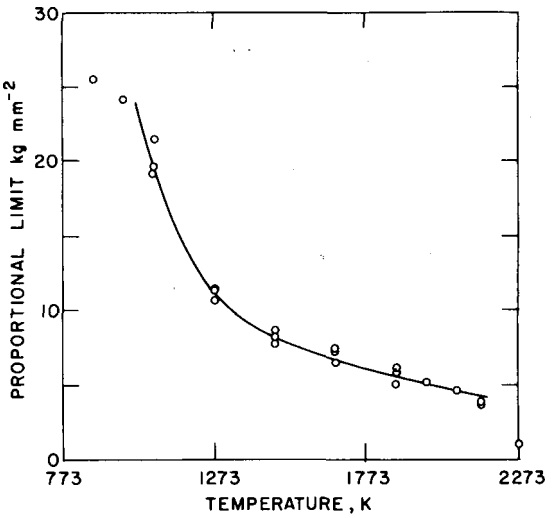

Figure 7. Temperature dependence of the proportional limit of $UO_{2.00}$.

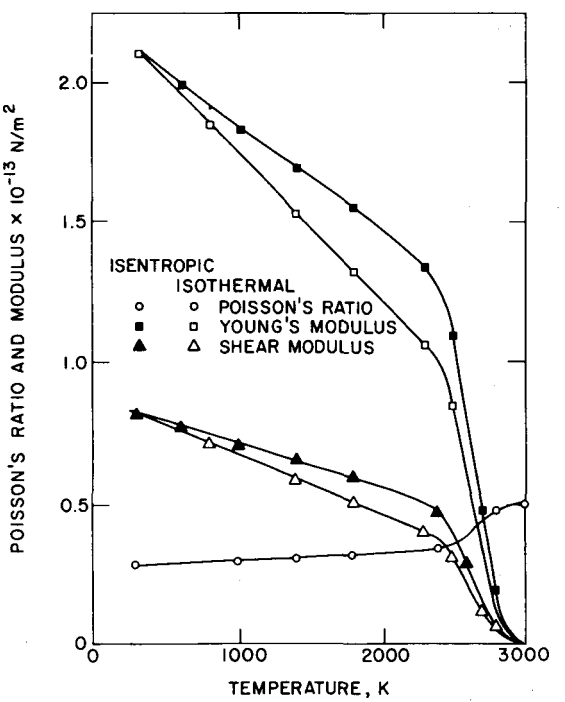

Figure 8. Poisson's ratio, Young's and Shear moduli as a function of temperature for recommended bulk modulus for Pu_2UO_2.

Bohaboy et al.[28] have measured the compressive creep behavior of the fuel and an empirical equation has been reported to describe strain rates for temperatures up to 2023 K. The general form of the equation is:

$$\dot{e} = A\sigma \exp(-Q_1/RT) + B\sigma^{4.5} \exp(-Q_2/RT) \quad (3.3)$$

where $\dot{e}$ = creep rate/hour

$A = 6.707 \times 10^{7}/(-87.7 + D)\, G^2$

$B = 9.488 \times 10^{-4}/(-90.50 + D)$

σ = compressive loading, KN/m^2

R = 1.986 Cal/mole/K

T = temperature, K

D = % of theoretical density (92 to 98)

G = grain size, microns (4 to 35)

$Q_1 = 3.768 \times 10^{5}$ J/mole

$Q_2 = 5.527 \times 10^{5}$ J/mole

In Slagle's work[28], this equation was extrapolated to 2773 K for comparison with high temperature experimental data. The comparison is shown in Figure 9. The calculated values (by Equation 3.3) are in excellent agreement with the measured values. Equation 3.3 can thus be used with confidence to determine fuel creep rates under high temperature conditions.

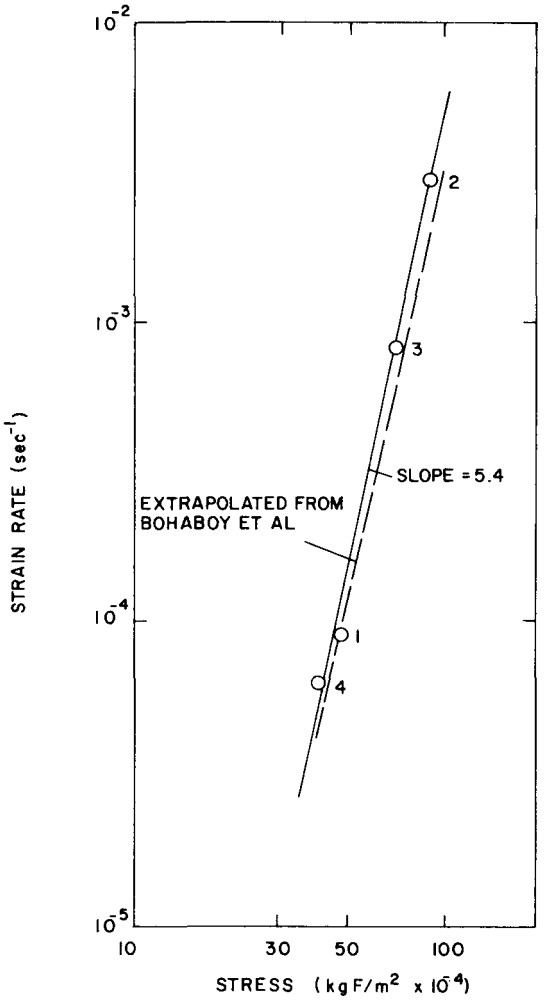

Figure 9. Strain rate versus stress for creep measurements made on UO_2 at 2773 K.

When the weight of fuel and other structures in the fuel rod (such as the cladding, end cap, gas tag capsule, spring in gas plenum and wire wrap) are taken into account and assumed to be exerted on the fuel column, it is calculated that, at the core midplane, the pressure on the fuel column is about 158.6 KN/m^2 (23 psi). At the bottom of the fuel column, this pressure is about 206.9 KN/m^2 (30 psi).

If we further assume that the irradiation-induced material swelling closes the clearance between fuel rods and the subassembly duct walls, then the weight of subassembly structures is also supported by the fuel columns after a partial meltdown of the duct wall. In this case, the pressure on the fuel columns would be about 379.2 KN/m^2 (55 psi) at the core midplane, and about 448.2 KN/m^2 (65 psi) at the bottom of the core.

These calculated pressures are obviously much smaller than the yield stress of the fuel material at temperatures below 2273 K. This indicates that the fuel column is not likely to slump (due to plastic deformation) under these loads at temperatures below 2273 K.

At temperatures higher than 2273 K, fuel slumping is assessed with creep rates determined by Equation 3.3. By using the calculated heating rate of the fuel during the loss-of-heat-sink accident that is presented in Section 4, the change of the fuel length, due to creep under compressive loading is calculated. The result is shown in Figure 10. Due to the loading by subassembly structures and fuel rod structures on fuel columns, the rate of fuel slumping is slow when the temperature is below 2673 K. Although this slumping rate increases above 2673 K, the calculated distance of slumping is only about 7.5 mm at 2973 K. This corresponds to a change of fuel column length of 0.8% which would not result in significant reactivity insertion (See Section 4.3).

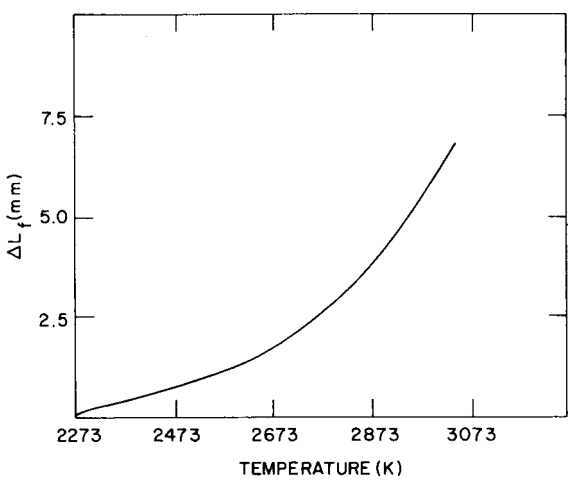

Figure 10. Change of fuel length under compression of upper structures.

3.3.2 Toppling Effect

After cladding meltdown, fuel columns lose their radial constraints. The void fraction in the active core region above the molten steel level increases from the originally designed value of 0.42 to about 0.65, due to the removal of steel structures. This enlarged voiding fraction enhances the likelihood of fuel pellet relocation due to toppling. Furthermore, under this circumstance, there are more than 39000 exposed fuel pellets piled into 217 columns in one fuel assembly. The possibility for solid fuel pellets to be relocated, due to toppling after cladding meltdown, cannot be ruled out without an assessment of destabilizing stochastic forces on the fuel pellet columns. For example, as shown in Figure 11, the diameter of these exposed fuel pellets (D = 4.9 mm) is only about double of the distance (Δ = 2.3 mm) between pellets on a line connecting original pellet centers. Movement of certain portions of only two fuel columns in one direction may allow an adjacent third column to collapse due to toppling (as illustrated in Figure 11). Other combinations of lateral and rotational motion of pellets could also cause the columns to topple.

If the duct wall melts down before the fuel columns collapse, additional constraints are lost and the possibility of fuel collapse, due to toppling, is further increased. Thus, possible scenarios of more condensed solid fuel configurations should be considered for recriticality assessment even though the fuel temperature (during this period of time) is still not high enough to allow for fuel slumping.

3.4 Control Material Fragmentation

Because of the relatively low temperature and temperature gradient in the control rod, the gas bubbles in the control material are small.[24] During the loss-of-heat-sink accident, these gas bubbles can be heated-up and

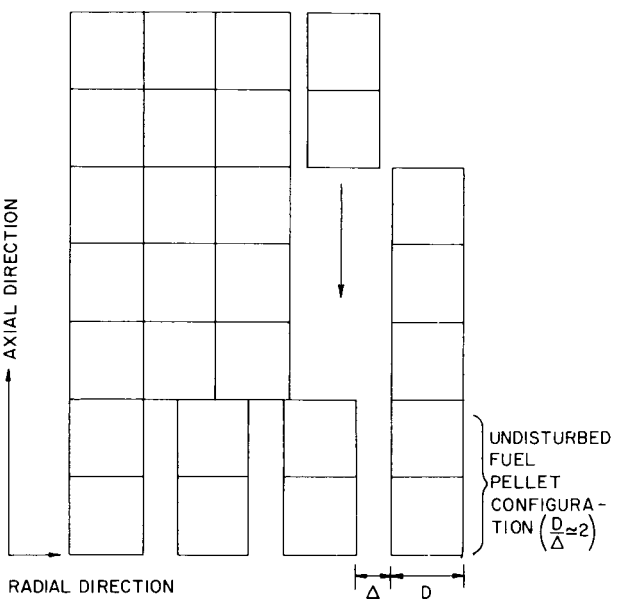

Figure 11. Illustrative scheme for toppling and D/Δ ratio for undisturbed bare fuel columns.

pressurized. It was assessed from the data in Reference 24, that for a control rod at 3% B^{10} burnup, the average bubble size could be about 1200 $\mathring{A}$ and the bubble concentration could be about 0.5×10^{11} bubbles/mm^3. By using these estimated numbers, the moles of gas atoms trapped in the bubble and the resulting pressure can be calculated. It is assessed that, before the material melts, the bubble pressure could be higher than the fracture stress of the control material. It is thus believed that it is possible that control material fragmentation will occur, due to the gas bubble pressurization, before the material melts.

4. ACCIDENT SEQUENCES AND RESULTS

The previous sections contain the models developed to describe the heat-up, meltdown, premelt failure and recriticality potential of the fuel and absorber pins within the voided core region. In this section, the results of our analysis are presented. In Section 4.1, the heat-up, meltdown, and relocation of the steel from the voided core region is considered. As the steel is removed from the core region, the potential for premelt relocation of the fuel or absorber material is assessed in Section 4.2. A number of nonmechanistic relocation configurations were assumed at various stages of steel meltdown. The configurations were chosen to envelop all plausible collapsing core scenarios. These configurations form the basis of the recriticality assessment presented in Section 4.3.

4.1 Accident Sequences

The LOHS code was developed to describe the heat-up of the core and the relocation of molten steel. Initially, the LOHS code was run without considering steel relocation so that the post-dryout heat-up phase could be described without the complication of material relocation. The results are presented in Section 4.1.1. The LOHS code was then run with steel relocation (Section 4.1.2) to determine if a steel plug could be formed as a result of clad melting, relocation, and refreezing. The position and extent of the steel plug affects subsequent fuel motion (Section 4.2) and has an impact on the potential for recriticality (Section 4.3).

4.1.1 Post-Dryout, Heat-up Phase

The meltdown progression was assessed using the LOHS code without considering material relocation (i.e., with the RLOCATE subroutine decoupled). The

results for the central axial node are presented in Figure 12, and may be compared with the simple hand calculations reported previously in Reference 8. Differences between the event times reported in Reference 8, and the data in Figure 12, is due to more realistic heat transfer modeling and the use of a computer code (LOHS) in the present assessment.

The data presented in Figure 12 indicates that all of the steel will be melted from the core region, substantially, before either the fuel or absorber material reaches their respective melt temperatures. Under these circumstances, with all of the steel support structure removed from the core region, the potential for premelt relocation of either the fuel or the absorber material must be considered (Section 3).

4.1.2 Clad and Duct Wall Relocation

The RLOCATE subroutine was coupled to the LOHS code, and the steel meltdown and relocation from the voided core region was predicted for a decay power level of 1% of full power. The sensitivity of the relocation model to axial node size and time step was reported in Reference 9, and it was determined that for an axial nodal structure greater than 60 nodes, and for time steps less than 0.1 seconds, the time to plug and the position of the plug were relatively insensitive to further changes in these two input parameters. Based on this sensitivity study, 64 axial nodes were selected together with a time step of 0.1 seconds. This corresponds to an effective relocation speed for the molten steel of 0.25 m/s. The event times, based on the above node and time step size are summarized in Table II.

It may be seen in Table II that meltdown of the fuel assembly clad begins 9.4 minutes after dryout and the first steel plug is formed at the bottom of the axial blanket after 13.4 minutes. The steel melting from the core region

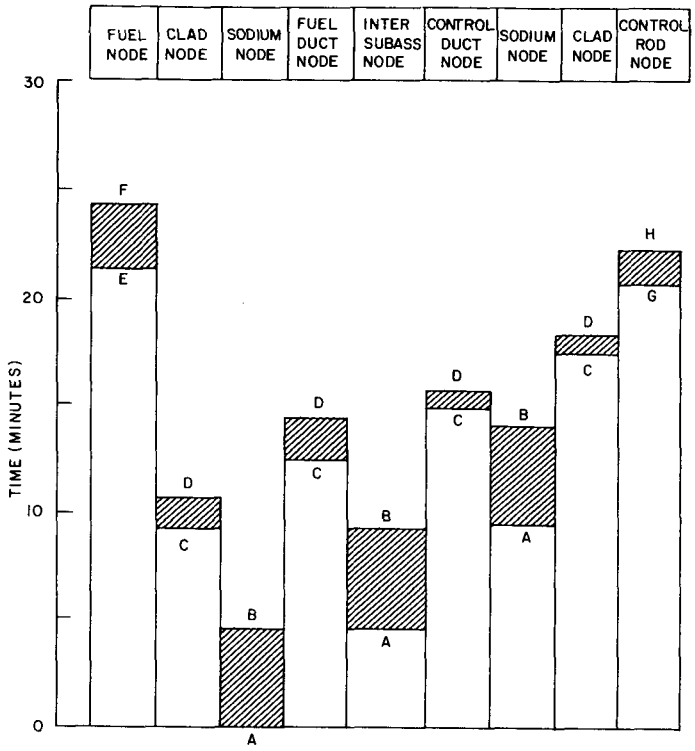

Figure 12. Meltdown progression for a LOHS after shutdown.

Table II
Clad and Duct Wall Relocation Positions
and Times to Plug

Material Melting	Start of Melt		First Plug Formed	
	Node*	Time Seconds (Minutes)	Node	Time Seconds (Minutes)
Fuel Clad	32	564 (9.4)	1	802 (13.4)
Fuel Duct Wall	32	768 (12.8)	1	839 (14.0)
Control Duct Wall	32	923 (15.4)	1	951 (15.9)
Control Clad	32	1089 (18.2)	24	1106 (18.4)

*There are 64 nodes through the active core and the axial regions. Node 1 is at the bottom of the lower axial blanket.

eventually builds-up the plug in the fuel assembly over the whole of the blanket region. Melting of the fuel assembly duct wall occurs 12.8 minutes after dryout. The duct relocates into the intersubassembly gap and causes a plug at the elevation of the lower axial blanket. The control assembly begins melting 15.4 minutes after dryout and forms a plug between the intact duct wall and the first row of the control pins at the elevation of the lower axial blanket. Finally, melting of the control assembly clad is predicted to occur 18.2 minutes after dryout. The lower gas plenum region of the control assembly is protected against heat transfer by the steel plugs formed from fuel clad and duct wall meltdown. As the temperatures in the lower gas plenum region of the control assembly are relatively low and the void fraction in which the molten clad can relocate is limited, the first steel plug is predicted to occur in the lower region of the absorber material. Subsequent molten steel relocation and heat exchange gradually cause the control cladding to settle in a configuration similar to the fuel assembly. The recriticality assessments (Section 4.3) are based on this steel meltdown configuration.

4.2 Possible Scenarios of Core Reconfiguration

In Sections 4.1 and 3, the time sequence of core meltdown progression and high temperature properties of fuel and absorber materials have been assessed. According to these assessments, accident progression has been addressed as shown in Figure 13.

As shown in Figures 12 and 13, at about 14 minutes after the saturation temperature is reached, the clad and duct wall in the fuel assembly are melted down, while those in the control assembly are intact. Around this time, the fuel temperature is about 2200 K. According to the assessment in Section 3.1, this

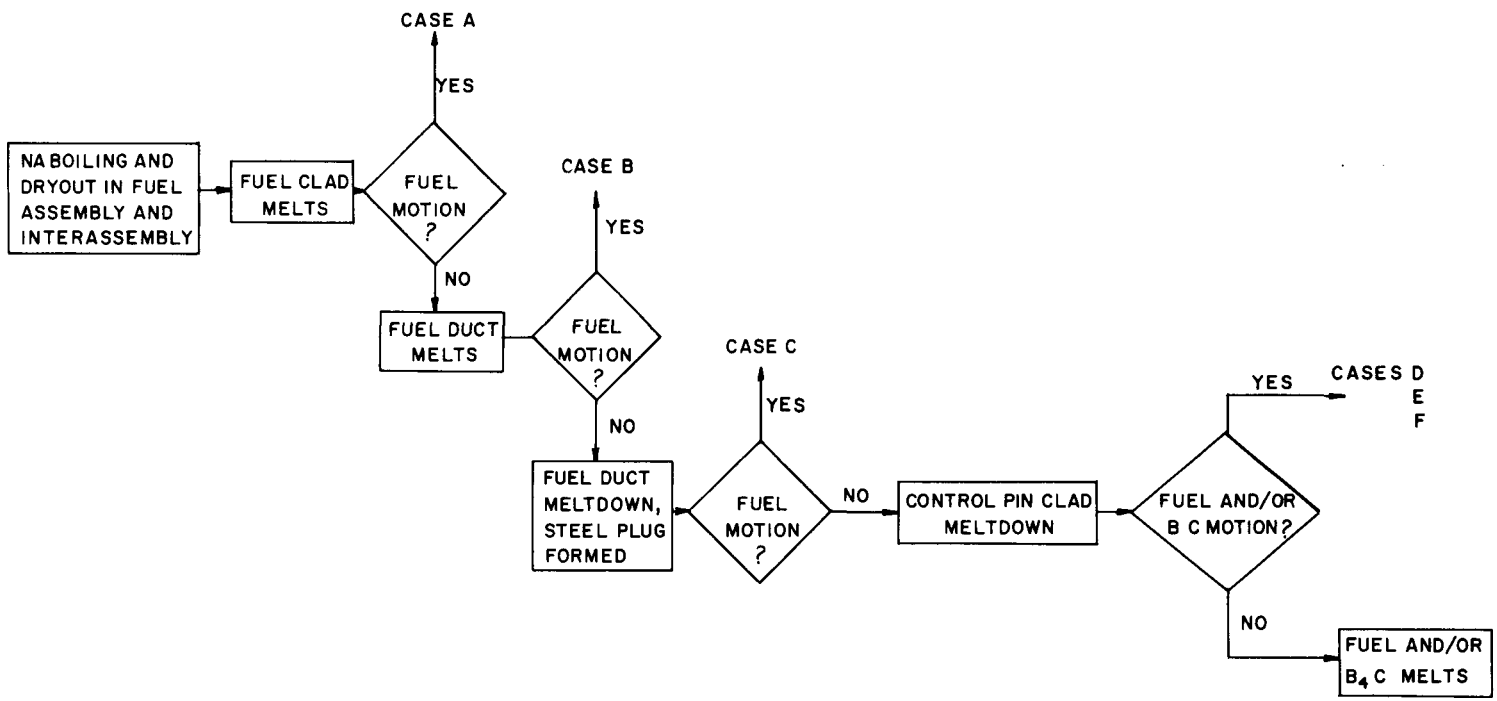

Figure 13. Accident scenarios and cases considered for material relocation and recriticality.

fuel temperature is not high enough to allow fuel slumping, due to possible loading of upper structures on fuel columns. But, because fuel columns lose radial constraint after cladding and/or duct wall meltdown, fuel material may be reconfigured due to toppling. As shown in Figure 13, three cases (namely: Cases A, B, and C) include possible fuel reconfiguration at different stages of the core meltdown process. The duct wall of the fuel assembly is assumed either to be intact, in the process of melting, or refrozen as a plug in the lower blanket for these cases, respectively. Evaluations of reactivity insertions for these cases are presented in Section 4.3. A brief description of Cases A, B, and C is shown in Table III.

After the melting of the duct wall in the control assembly, there are more than five minutes before the melting of fuel and absorber materials (Figure 12). As discussed in Section 4.1, during this time-period, stainless steel plugs are formed in the lower gas plenum region of the control assembly. After the melting of cladding in the control assembly, the control material may be relocated due to toppling. In high burnup control assemblies, the control material has a significant potential to fragment (See Section 3.2) and can thus relocate more extensively. Because the relocation of control material occurs, in general, after meltdown of the cladding and duct wall, and the density of control material is about one-third (1/3) of molten stainless steel, the bulk of the relocated control material will rest on top of the relocated stainless steel.

After the meltdown of cladding in the control assembly, the fuel temperature is rather high. At about one minute before the start of fuel melting, the fuel temperature is within 100 K of its melting temperature. During this

Table III

List of Cases for Recriticality Calculations

	FUEL ASSEMBLY	CONTROL ASSEMBLY
CASE A	SODIUM DRYOUT, CLADDING MELTDOWN, FUEL COLLAPSE	INTACT
CASE B	CASE A WITH DUCT WALL MOLTEN AND SLUMPED ALONG WITH FUEL	INTACT
CASE C	CASE A WITH DUCT WALL STEEL RELOCATED AS PLUG BELOW CORE	INTACT
CASE D	AS IN CASE C BUT WITH-OUT FUEL COLLAPSE	CLADDING & DUCT WALL MELTDOWN, B_4C COLLAPSE
CASE E	CASE D WITH FUEL COLLAPSE	CASE D WITH A B_4C COLLAPSE OF 0.2M
CASE F	CASE D WITH FUEL COLLAPSE	CASE D WITH A B_4C COLLAPSE OF 0.3M

time-period, as discussed in Section 3.1, the fuel column can be reconfigured, not only by toppling, but also by slumping due to possible loading by upper structures.

Thus, after meltdown of the duct wall in control assemblies, fuel and control materials may move together or sequentially (Figure 13). Combinations of their movements result in reactivity changes. Parametric cases (Cases D, E, and F) for the recriticality study with different combinations of material relocations, are described briefly in Table III.

As we can see in Figure 13, fuel and control materials will melt even if recriticality is not attained. Results calculated for Cases D, E, and F are also valid recriticality assessments for fuel and/or control material relocations due to melting (prior to any direct mixing of fuel and control materials).

4.3 Potential for Recriticality

4.3.1 Configurations Analyzed

The possibility of a recriticality following a loss-of-heat-sink accident is dependent on the sequence of events after the fuel material starts collapsing. At the point in time when the fuel material starts collapsing, it is assumed that the core is voided of sodium; most, or all of the steel is removed from the core and the control rods are fully inserted. The steel forms a plug in the lower axial blanket and core. This configuration is subcritical, since the negative reactivity effects, due to the control rods, Doppler feedback, and axial expansion are larger than the positive reactivity effects due to sodium and steel removal. If at this point the material collapses without mixing, a point will be reached when a critical configuration will be achieved. This assumed mode of collapsing is conservative since the upper axial blanket material might mix with the remaining core material, thus making recriticality less

likely. In all the scenarios considered in these calculations, no mixing of fuel or absorber materials across boundaries between adjoining regions was considered. Additionally, it was assumed that all fuel and absorber material motions are axial.

The core configuration considered as the starting point for the accident is assumed to be a beginning-of-life core[16]. This is a conservative starting point for the currently proposed accident sequence, since no fission products are accounted for. Three different geometric configurations were considered and they are illustrated in Figures 14-16. The first two scenarios (Cases C and B) are similar, their only difference being the mass of steel remaining in the core and the size of the steel plug. The third scenario (Case D) involves the collapse of control rods prior to the collapse of fuel. In addition to the above three scenarios, scenarios which are combinations of fuel and control material slumping were also analyzed. Finally, a scenario (Case A) was considered which is a slight modification of the one shown in Figure 15; in this case, the subassembly duct walls are assumed to remain intact during fuel collapse. This implies that the amount of steel within the compacting core is reduced in comparison to the Case B scenario.

Figure 14 is an illustration of the Case C scenario. Materials 1 and 2 are the axial and radial blankets, respectively, material 4 is the inserted central control rod, and material 11 represents the inserted control rods in the upper axial blanket. These materials are unchanged from the base case and are thus carried over directly from it. Materials 3, 5 and 7 are portions of the lower axial blanket, the inner core and the outer core, respectively, with all the sodium removed and replaced by steel. This steel represents the

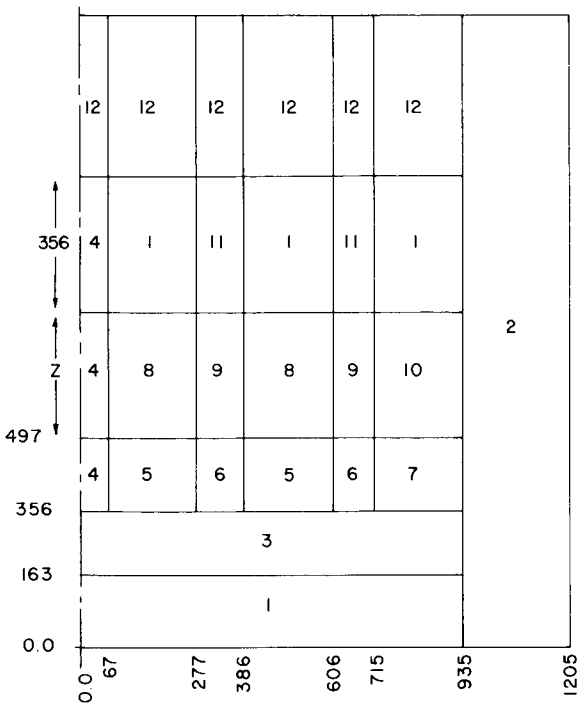

Figure 14. Scenario C (indicated distances in millimeters).

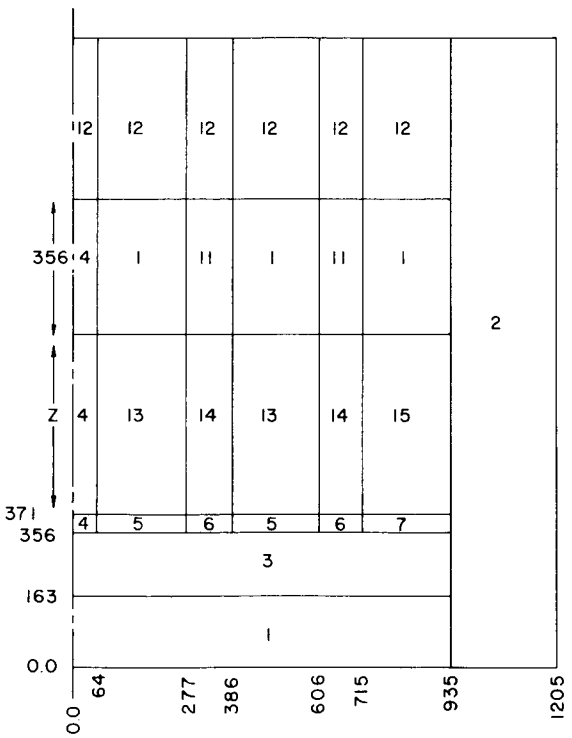

Figure 15. Scenario B (indicated distances in millimeters).

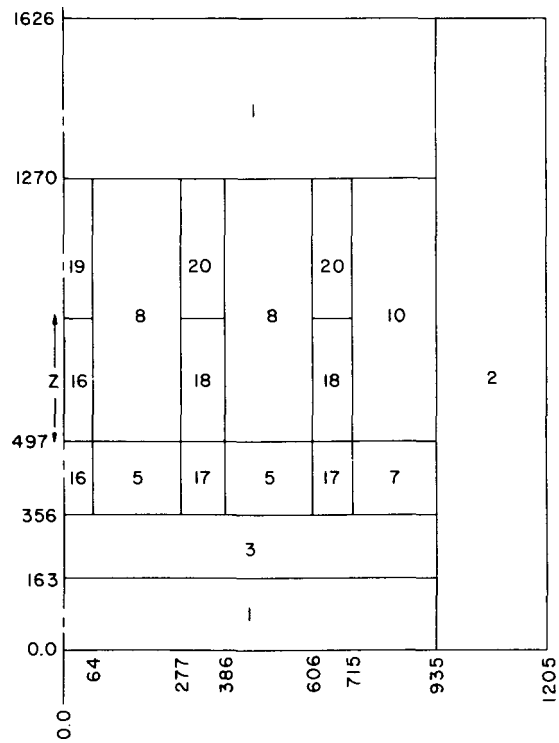

Figure 16. Scenario D (indicated distances in millimeters).

steel plug which forms in the lower axial blanket and core. Material 6 represents the control rod rings which are fully inserted and is a mixture of materials 4 and 5. Materials 8 and 10 are the inner and outer core fuel, respectively. There is no sodium or steel present in this mixture, and there is no cross-mixing between the inner and outer core.

The height Z is varied and in this way the postulated compaction is simulated. Material 9 represents the inserted control rods in the region which is the appropriate mixture of region 8 and region 4. Material 12 is a low density iron reflector, representative of the structural material in this region.

Figure 15 illustrates the Case B scenario which was analyzed. The difference between this scenario and Case C is the reduction of the steel plug thickness from 0.33 m to 0.2 m and the introduction of the remaining steel into the core region above the plug. Materials 13 and 15 are thus similar to materials 8 and 10 except that the appropriate amount of steel is added to them. Finally, material 14 is representative of the control rod ring at this position and is a mixture of materials 10 and 4.

A second scenario, based on Case B was also considered. This scenario is known as Case A and assumes that the duct walls do not form part of the collapsing core, but remain intact. As pointed out above, the effect of this assumption is to reduce the fractional mass of steel present in the core, and thus the composition of the core materials 13, 14, and 15 had to be appropriately modified.

Figure 16 illustrates the Case D scenario in which it is assumed that the control rods, rather than the core, collapse. It is further assumed that the steel and sodium present in the control subassemblies (clad and duct wall) have all relocated. The start of this accident is thus essentially

identical to the beginning of the Case C scenario. As the accident sequence progresses, the control rod height Z decreases, implying shorter, but more highly compacted control elements. The primary difference between Case D and Case C are the materials 16, 17, 18, 19, and 20. Materials 16 and 19 are the compacting central control rod and vacuum, respectively. Materials 17 and 18 are an appropriate mixture of the compacting control rod rings and the core regions 5 and 8. Finally, material 20 is a reduced density representation of Material 8, the reduction in density accounting for the missing control subassemblies.

4.3.2 Recriticality Results

Using the method described in Section 2.3 and models mentioned above, calculations were carried out for different control rod and active-core heights. The active core is defined as the distance between the upper axial blanket-core interface and the lower axial blanket-core interface. A range of active-core heights between 0.41 m and 0.91 m, and a range of control rod heights between 0.35 m and 0.91 m were considered. The lower height in each case corresponds to a material density with no voids, and 0.91 m corresponds to the full core height.

The results of these calculations are illustrated in Figures 17-19. Figure 17 shows the variation of the multiplication factor (k_e) for various core heights and for different scenarios. In all these cases, the control rods were not moved and remained at their full height of 0.91 m. Case C, which has a minimum amount of steel in the active core, shows the highest values for k_e. In Case B, the assumption is made that the subassembly steel stays in the core and compacts along with it, and consequently, the values of k_e are seen

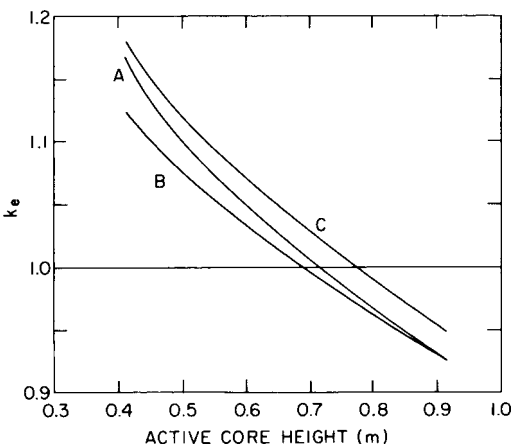

Figure 17. k_e versus collapsed core height.

to be significantly lower. Finally, in Case A, the subassembly duct walls are assumed to remain in place, but do not collapse. Thus, the fractional steel content of the active core starts at the same value as in Case B, but asymptotically approaches that of Case C. For this reason, the value of k_e for Case A varies in a similar manner, i.e., starts at Case B and asymptotically approaches Case C. Figure 18 shows the variation of k_e with control rod height (Case D). In this case, the core material is assumed to remain at the full height (0.91 m). The value of k_e is seen to rise slowly, initially, and eventually more rapidly. It is seen that for all cases illustrated on Figures 17 and 18, the possibility exists for achieving a critical mass.

In addition to the above two scenarios, a third set (Cases E and F) of calculations was carried out. These configurations assumed a precompacted control assembly, and then the fuel was compacted to achieve a critical mass. In this way, the change in reactivity, due to simultaneous collapse of fuel and control assemblies at different times and/or rates, can be estimated. Figure 19 shows a contour plot of active-core height and control subassembly height for k_e=1. It is seen that a large area of the map is excluded due to compaction limits. Furthermore, it is seen that within the limits of the current model, no configuration could reach these limits without passing through the k_e=1 contour. Figure 19 illustrates that for any fuel compaction greater than 0.12 m, regardless of the amount of control rod compaction, the reactor will become critical. Since the fuel material will ultimately relocate downward (in a solid or molten state), the conclusion that recriticality will occur appears to be unavoidable.

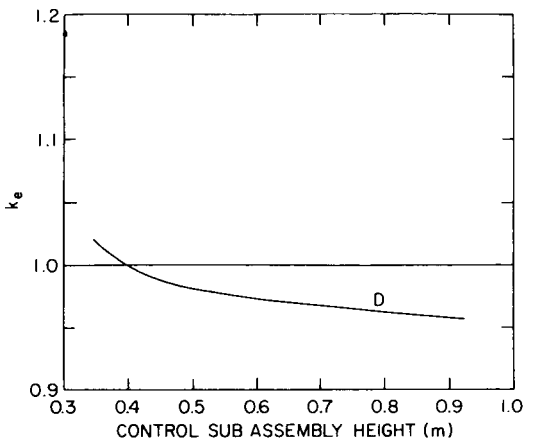

Figure 18. k_e versus collapsed control material height.

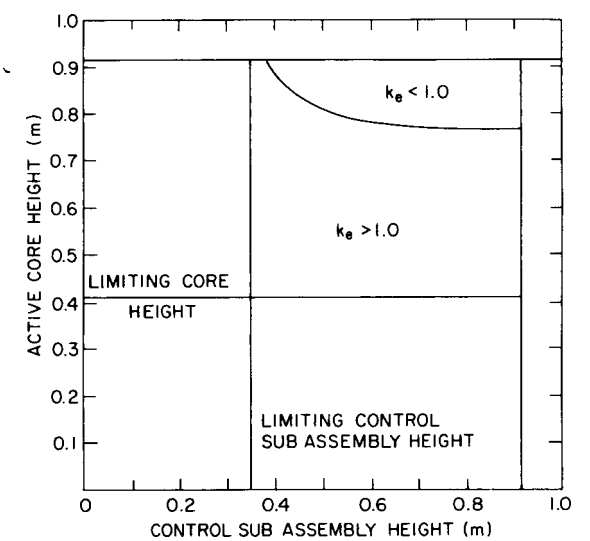

Figure 19. Contour of k_e = 1.

4.3.3 Limitations on Criticality Techniques

The likelihood that the scenarios, as currently envisaged, being valid as k_e reaches unity will be small. This is due to the fact that fairly large core motions are required and the assumption that there be no mixing both radially and axially, would probably break down. Any dilution of the core material by axial blanket material (^{238}U, Steel, Na) or control assembly material (^{10}B, ^{11}B or Carbon) would have the effect of reducing k_e. On the other hand, mixing outer core material into the inner core space would increase the value of k_e.

Finally, it should be pointed out that the calculational techniques used are subject to the following two approximations:

1. The cross-section library (50 groups) was created for a typical LMFBR core. Thus, the spectrum over which they were collapsed did not allow for any compaction and voiding of sodium and steel.

2. Only P_0 (transport corrected) scattering was used. It is believed that higher order scattering moments might be necessary, since the spectrum will harden due to sodium and steel voiding, making the inclusion of higher order scattering more desirable.

Despite the shortcomings of the calculational techniques, it is believed that the overall trends indicated by the analysis are valid.

5. SUMMARY AND DISCUSSION

5.1 Summary of Results

The foregoing analysis of the loss-of-heat-sink accident can be summarized as follows. The initiator of the accident was a total loss of heat sink after neutronic shutdown at the intermediate heat exchangers, followed by a loss-of-electrical power to the primary heat transport system pumps. While these are not necessary conditions for a core meltdown, they are sufficient for the purposes of forcing a meltdown and of simplifying the considerations of pre-dryout, two-phase sodium flow analysis.

After sustained dryout of the clad, which occurs in not less than 3.3 hours after shutdown, the remainder of the accident is conveniently measured in minutes (recriticality is expected to occur within approximately twenty minutes).

It was found that the following phenomena influence the course of events during the meltdown and relocation phases of the accident:

a) downward relocation and refreezing of fuel pin cladding, fuel assembly duct walls, control pin cladding and control assembly duct walls;

b) radiative heat transfer between the fuel and control assemblies;

c) bare fuel and/or absorber pellet column instability and the potential for material fragmentation.

It was found that the following phenomena were of rather less importance for these phases of the accident:

a) the impact of fission gas release from the fuel pins and Helium gas release from the control pins on the heat transfer processes and material relocation;

b) compression of fuel and/or absorber pellets due to transient loading by upper structures;

c) sodium vapor streaming velocities.

Although a great quantity of steel was relocated from the core space to a region just below the active core elevation, the reactor remained subcritical (sodium was voided from the core space as well) until sufficient fuel and/or absorber material motion occurred.

The approach taken to assess the potential for recriticality was basically an event tree scheme in which branches were developed at points of technological uncertainty with regard to material motion in the disrupted core. Each branch ended with a determination of the neutronic behavior of the particular disrupted configuration. It was significant to this study that all branches ended at a recritical reactor and, therefore, recriticality appears to be a necessary event in the loss-of-heat-sink accident sequence. The accident was not taken beyond the point of recriticality but it was expected, due to the slowness of the relocation process, that the subsequent material motion will be benign.

5.2 Unresolved Problems

As suggested above, an assessment of the further course of events for this accident would involve an analysis of coupling between the neutronic behavior and the disrupted material motion. This analysis would be necessary before the accident sequence can be extended towards the post-accident heat removal phase. In connection with the latter, it would be necessary to determine (or postulate) the mode of restoration of the heat sink. For example, a heat sink may become available to the core debris with the primary system intact or the debris may come into a coolable configuration outside the reactor vessel.

In any case, issues related to post-accident heat removal would require further in-depth analysis and must, according to the present state-of-the-art, rely on parametric, scoping procedures.

Although the accident analysis presented here was carried out for a specific loss-of-heat-sink accident (idealized to assure core-meltdown), it is believed that much of the work is somewhat generic and that the conclusions are valid for a wider scope of initiators. Although the work of Chan et al.[7] lends support to this belief, further studies of the rather more likely initiators and their consequences may be warranted.

A key assumption of this work is that the sodium voiding of the core space is sustained during the period of approximately twenty minutes following fuel pin cladding dryout. If significant sodium re-entry could occur during this period, perhaps due to the restoration of forced circulation, then the accident sequence would be altered from that presented in this work.

Finally, we remark on the relevance of the foregoing work to potential loss-of-heat-sink accidents in alternative LMFBR designs. At the outset, it is hoped that future LMFBRs will be designed with sufficiently reliable shutdown heat removal systems to preclude the necessity for detailed studies of the accident progression. The study performed for the CRBR, although specific to a given reactor geometry, contains features that are generic. For example, the transient analysis of the control assembly response would be applicable to other LMFBR configurations undergoing a slow heatup transient.

For other LMFBR designs, factors which may lead to differences in the meltdown sequences are related to the presence of internal breeding blankets (parfait core designs) and in-core test assemblies (Fast Flux Test Facility). These assemblies can provide temporary heat sinks, which could in turn lead to

a less coherent meltdown and relocation pattern in the core. In addition, these assemblies may provide a mechanism for dilution of disrupted core debris if significant radial movement of materials occurs and, therefore, may influence the potential for recriticality.

REFERENCES

1. "Final Environmental Statement Related to the Construction and Operation of the Clinch River Breeder Reactor Plant," NUREG-0139, U. S. Nuclear Regulatory Commission, (February 1977).
2. "Reliability of the CRBRP Shutdown Heat Removal System," NEDM-14082, General Electric Corporation, (January 1976).
3. A.J. Buslik, I.A. Papazoglou, and R.A. Bari, "Reliability of the Shutdown Heat Removal System of the CRBR," BNL-NUREG-21962, Brookhaven National Laboratory, (October 1976) and Proceedings of the Topical Meeting on Probabilistic Analysis of Nuclear Reactor Safety, Vol. 2, p. V.2-1, May 8-10, 1978, ISBN: 0-89448-1010.
4. IAEA Meeting of Specialists on the Reliability of Decay Heat Removal Systems for Fast Reactors, Harwell, England (Summary Report), (April 1975).
5. Reactor Safety Study, WASH-1400, U. S. Nuclear Regulatory Commission, (October 1975).
6. H.K. Fauske, Trans. Am. Nucl. Soc., 22, 385 (1975); S. H. Hakim and R. J. Henninger, Trans. Am. Nucl. Soc., 24, 261 (1976).
7. C.K. Chan, T.K. Min and D. Okrent, "A Look at Alternative Core Disruption Accident in LMFBR's," UCLA-ENG-7720, (February 1977).
8. R.A. Bari, M.A. Klenin, W.T. Pratt and Y.H. Sun, "Preliminary Assessment of the Meltdown Progression of the Loss-of-Heat-Sink Accident with Scram in the LMFBR," BNL-NUREG-23137, (August 1977).
9. R.A. Bari, H. Ludewig, W.T. Pratt and Y.H. Sun, "Material Relocation and Recriticality Assessment for the Loss-of-Heat-Sink Accident in the LMFBR," BNL-NUREG-23432, (November 1977).

10. R.A. Bari, M.A. Klenin, W.T. Pratt and Y.H. Sun, Trans. Am. Nucl. Soc., 26, 347 (1977).

11. R.A. Bari, H. Ludewig, W.T. Pratt and Y.H. Sun, Trans. Am. Nucl. Soc., 28, 471 (1978).

12. D.C. Albright and R.A. Bari, "Loss-of-Heat-Sink in the Secondary Heat Transport System of the Fast Flux Test Facility," BNL-NUREG-23269, (September 1977).

13. LMFBR DEMO Plant Simulation Model (DEMO), WARD-D-0005 (Rev. 4) Westinghouse Electric Corporation, (February 1976).

14. S.H. Chan, D.W. Condiff and M.A. Grolmes, "Radiative Cooling of a Voided Subassembly," ANL-76-5, Argonne National Laboratory, (January 1976).

15. M.A. Grolmes, G.A. Lambert and H.K. Fauske, "Flooding Correlation for Sodium and Cladding Motion in Subassembly Voiding," Trans. Am. Nucl. Soc., Soc., 18, 209 (1974).

16. H. Ludewig and D. Majumdar, "Preliminary Investigation of Recriticality in the Transition Phase of Core-disruptive Accidents in the CRBR," Brookhaven National Laboratory, BNL-NUREG-21811, (September 1976).

17. R.B. Kidman et al., "LIB-IV, A Library of Group Constants for Nuclear Reactor Calculations," Los Alamos Scientific Laboratory, LA-6260 MS (1976).

18. C.R. Weisbin et al., "MINX - A Multigroup Interpretation of Nuclear X-sections from ENDF/B," Los Alamos Scientific Laboratory, LA-UR-1766.

19. R.B. Kidman et al., "CINX - Collapsed Interpretation of Nuclear X-sections," Los Alamos Scientific Laboratory, LA-6287-MS (1976).

20. R.W. Hardie et al., "1-DX - A One-Dimensional Diffusion Code for Gen erating Effective Nuclear Cross Sections," Battelle Memorial Institute, BNWL-954 (1969).

21. K.D. Lathrop et al., "TWOTRAN-II An Interfaced Exportable Version of the TWOTRAN Code for Two-Dimensional Transport," LA-4848-MS (1973).

22. A.L. Aronson, "TWOTRAN-II" a memorandum to M.M. Levine, Brookhaven National Laboratory (1975).

23. Preliminary Safety Analysis Report, Clinch River Breeder Reactor Plant, Project Management Corporation, Docket 50-537, June 1975, Sec. 4.2.

24. A. Jostsons et al., "Defect Structure of Neutron Irradiated Boron Carbide," J. of Nucl. Mat., 49, 130 (1973/74).

25. Y. Sun and D. Okrent, "A Simplified Method of Computing Clad and Fuel Strain and Stress During Irradiation," NUREG-0260, (June 1977).

26. J.F. Byron, "Yield and Flow of Polycrystaline Uranium Dioxide," J. of Nucl. Mat., 27, 48 (1968).

27. F.E. Bard et al., "A Thermoelastic Material Properties Correlation for Uranium/Plutonium Mixed Oxide," HEDL-TME 74-12, (February 1974).

28. P.E. Bohaboy et al., "Compressive Creep Characteristics of Stoichiometric Uranium Dioxide," GEAP-10054, (May 1969).

29. C.A. Burgess, W.H. Sheeley, "LMFBR Mixed-Oxide Fuels Development Semiannual Report," HEDL-TME 75-72, p. 77, January 1976.

ACKNOWLEDGMENTS

We gratefully acknowledge the technical contributions of M. A. Klenin, T. P. Henry and A. L. Swoboda to various stages of this work. We also thank D. C. Albright for helpful discussions of the DEMO code and of related information. Finally, we are indebted to J. F. Meyer of the U.S. Nuclear Regulatory Commission for his support, valuable comments, and encouragement throughout the course of this work.

NOMENCLATURE

Symbol	Description
A	area
C_{PX}	specific heat of material X
h_{fg}	latent heat of vaporization
M	mass
M_{BOIL}	mass vapor production
q	heat flux
Q	power, heat flow rate
t	time
T	temperature
T_m	melt temperature
u	velocity
Δ	incremental change
λ	latent heat of fusion
ρ	density
σ	Stefan-Boltzmann constant

Subscript	
F	Fuel Material
FC	Fuel Clad
FD	Fuel Duct Wall
CD	Control Duct Wall
CC	Control Clad
C	Absorber Material

NOMENCLATURE (Cont.)

Subscript	Description
i	defines radial node
INT	internal
j , J	defines axial node
R	radiation